



Full Text View

[Volume 28, Issue 12 \(December 1998\)](#)

Journal of Physical Oceanography

Article: pp. 2362–2381 | [Abstract](#) | [PDF \(307K\)](#)

A Geostrophic Vortex over a Slope*

Joseph H. LaCasce

MIT/WHOI Joint Program in Physical Oceanography, Woods Hole Oceanographic Institution, Woods Hole, Massachusetts

(Manuscript received March 27, 1997, in final form December 1, 1997)

DOI: 10.1175/1520-0485(1998)028<2362:AGVOAS>2.0.CO;2

ABSTRACT

Nonlinear, quasigeostrophic, f -plane vortices in two layers over a topographic slope are considered. Scaling arguments suggest two parameters that dictate the effective strength of the slope: the first indicates the likelihood of dispersion at depth, and the second relates to baroclinic stability. If the deep flow is only weakly dispersive (weak slopes), an initially barotropic vortex can translate barotropically across the isobaths, provided the vortex scale exceeds the deformation scale. Over stronger slopes, the vortex separates into topographic waves and a stationary, surface-trapped vortex. An initially surface-trapped vortex larger than deformation scale becomes unstable over a weak slope, as it does over a flat bottom. However, a strong slope can stabilize the vortex to small perturbations, despite the large vortex scale. The effective slope parameters depend not only on topographic grade, but on vortex strength and size, and on the ambient stratification. Parameters obtained with representative oceanic values suggest that topographically induced vertical decoupling may be quite common.

1. Introduction

It is well known that there are eddies in the ocean, and that these features are often quite large, energetic, and possess significant vertical structure. They are important in terms of local current variability, and perhaps to the lateral transport of momentum and tracers. Gulf Stream rings and Agulhas eddies are two notable examples: both are of the order of 100 km in scale, are baroclinic, and possibly transport heat in the North and South Atlantic Oceans. Eddies such as these often interact with topography, either the continental shelf, ridges and canyons or even isolated seamounts, which in turn may lead to drastic structural alterations, and perhaps even to destruction. As such, a complete understanding of how eddies redistribute properties requires a knowledge of how topography affects their dynamics. The present work seeks a broad understanding of the effect of topography on such vortices.

Table of Contents:

- [Introduction](#)
- [Equations and numerics](#)
- [Scaling](#)
- [Initial conditions](#)
- [A barotropic vortex](#)
- [A surface vortex](#)
- [Discussion](#)
- [REFERENCES](#)
- [TABLES](#)
- [FIGURES](#)

Options:

- [Create Reference](#)
- [Email this Article](#)
- [Add to MyArchive](#)
- [Search AMS Glossary](#)

Search CrossRef for:

- [Articles Citing This Article](#)

Search Google Scholar for:

- [Joseph H. LaCasce](#)

Observations of eddy–topography interactions are numerous. An eddy may be substantially weakened while passing over steep topography, as seen by [Cheney and Richardson \(1976\)](#) for the case of a cold core ring south of the Gulf Stream, and [Vidal et al. \(1994\)](#) with a Loop Current eddy in the Gulf of Mexico. Vortices may possibly break up after hitting steep relief; [Richardson et al. \(1989\)](#) were unable to relocate a “meddy” after it collided with a seamount and suggested that it might have been destroyed. Further, [van Ballegooyen et al. \(1994\)](#) suggest that Agulhas eddies are often blocked in their migration across the South Atlantic by the Walvis Ridge.

Previous theoretical works have considered different aspects of this interaction. Barotropic studies (e.g., [Wang 1992](#); [Grimshaw et al. 1994a](#)) suggest that a vortex may indeed disperse rapidly into topographic waves over strong slopes. On the other hand, barotropic eddies can translate across weak topography by self-induced motion, much like hurricanes can migrate in the atmosphere even in the absence of external wind forcing (e.g., [Adem 1956](#)). This was observed, for example, in the laboratory studies of [Carnevale et al. \(1991\)](#). Vortex drift across topography, and in particular the effect of a free surface, is also discussed in [Grimshaw et al. \(1994b\)](#).

However, eddies such as Gulf Stream rings are not barotropic and the ocean is stratified, so it is important to understand baroclinic effects. One of the earliest studies of a baroclinic eddy interacting with topography is that of [Smith and O’Brien \(1983\)](#). They considered various vortices in two layers interacting with a linear continental slope. They pointed out that the topography only affected the vortex if there was flow initially in the lower layer. [Kamenkovich et al. \(1996\)](#) similarly studied the effect of a submarine ridge on a translating surface eddy, such as an Agulhas eddy. They found that 1) the eddy tended to adjust to a compensated state (zero deep flow) after impacting the ridge and 2) that the strength of the deep flow prior to impact determined the degree of interaction. Vortices that had strong deep flows suffered a strong interaction, and were possibly destroyed. Sakamoto and Yamagata (1996) also consider a baroclinic vortex translating over an isolated obstacle from the perspective of the so-called JEBAR effect. Finally, topography may also affect the baroclinic stability of a vortex, as demonstrated in the linear stability analysis of [Hart \(1975\)](#). He found that a weak slope could destabilize a surface-trapped vortex, but that strong slopes suppress unstable growth.

Studies of stratified vortices (e.g., [McWilliams and Flierl 1979](#); [Mied and Lindemann 1979](#)) on the β plane are also relevant to vortices over weak slopes, as discussed below. And studies of the generation of topographic waves over the continental shelf by ringlike structures (e.g., [Louis and Smith 1982](#); [Shaw and Divakar 1991](#)) are also closely related.

The present work seeks a broad categorization of nonlinear baroclinic vortex evolution over topography. Specifically, I will characterize the vortex adjustment over weak and strong slopes with weak and strong stratification. It is argued that two elements are of fundamental importance: the rate of topographic wave dispersion and vortex stability [which is altered by topography, as suggested by [Hart \(1975\)](#)]. The relative importance of each effect may be gauged by two nondimensional parameters, found by scaling. An a priori knowledge of these parameters generally permits the prediction of the qualitative aspects of the evolution, if not the quantitative changes as well.

To limit the possibilities, only two types of initial vortex are considered: an initially barotropic vortex and one initially surface trapped. Of course there are other possibilities, but the aforementioned phenomena are arguably best observed with such vortices. Moreover, these choices permit comparisons with previous barotropic studies, and with the stability analysis of [Hart \(1975\)](#). It is argued that more general initial profiles yield a combination of the responses identified here.

The equations and numerical method are described in the next section, followed by the scaling and a description of the initial conditions. Two specific examples are considered thereafter to probe the parameter dependence. Concluding remarks, and a discussion of observed eddies, follow.

2. Equations and numerics

As noted, the model employs two layers, quasigeostrophic (QG) dynamics, and a linear slope. For the sake of simplicity, the planetary gradient is assumed to be zero; that is, $\beta = 0$. The implications of this omission are discussed a posteriori. Quasigeostrophy implies a small Rossby number, small interface displacements, and weak topographic slopes ([Pedlosky 1987](#)), and so is not strictly valid for oceanic regions with fronts and/or strong bottom slopes. However, as argued below, it is still possible to obtain strong topographic *effects* with this system, which permits fast topographic waves.

The QG equations are more computationally efficient than the primitive equations, permitting higher horizontal resolution and so decreased lateral damping. Also, because equations for potential vorticity (PV) are employed, rather than momentum equations, it is possible to include a mean PV gradient in a doubly periodic domain, that is, one without lateral boundaries. The lack of lateral boundary layers simplifies the solution, but the intended oceanic region is thus necessarily far from coasts.

Assuming a slope that shoals in y , the inviscid equations for the layerwise PV are (e.g., [Pedlosky 1987](#))

$$\frac{\partial}{\partial t} q_1 + J(\psi_1, q_1) = 0 \quad (1)$$

$$\frac{\partial}{\partial t} q_2 + J(\psi_2, q_2) + \beta_2 \frac{\partial}{\partial x} \psi_2 = 0 \quad (2)$$

with $q_i \equiv \nabla^2 \psi_i + F_i (\psi_{3-i} - \psi_i)$ the perturbation potential vorticities and ψ_i the streamfunctions for layers $i = 1, 2$. The Jacobian is defined as

$$J(a, b) \equiv \left(\frac{\partial a}{\partial x} \frac{\partial b}{\partial y} - \frac{\partial b}{\partial x} \frac{\partial a}{\partial y} \right)$$

and ∇^2 the horizontal (two dimensional) Laplacian operator. The (squared) inverse of the deformation radius in each layer is $F_i = f^2 / (g' H_i)$ with g' the reduced gravity, f the Coriolis parameter, and H_i the depth of the layer. The layer depths are assumed to be equal so that $F_1 = F_2 \equiv F$, unless indicated otherwise.

The linear slope yields a constant background PV gradient [“topographic beta,” e.g., [Faller and VonArx \(1955\)](#)] of magnitude $\beta_2 \equiv -f(\partial_y H_2) / H_2$, which is only present in the lower layer. As such, q_1 is conserved on fluid parcels, but q_2 is not, and changes as parcels move across isobaths. However the “total PV” in layer two ($q_2 + \beta_2 y$) is conserved on parcels.

[Equations \(1\)–\(2\)](#) were solved with the Fortran code used in [Flierl \(1994\)](#). All variables are Fourier decomposed in both directions:

$$(\hat{q}_i, \hat{u}_i) = \frac{1}{N_x N_y} \sum_{k=k_{\max}+1}^{k_{\max}} \sum_{l=l_{\max}+1}^{l_{\max}} (q_i, u_i) \exp(ikx + ily), \quad (3)$$

where $N_x = N_y$ are the number of Fourier modes. The domain size is taken to be $2\pi \times 2\pi$, a common choice which yields integral wavenumbers and $(k_{\max}, l_{\max}) = (N_x/2, N_y/2)$. Variables are alternately referred to by their Fourier and real representations, and the hat distinguishes the Fourier transform [as in [\(3\)](#)]. Generally 64^2 or 128^2 modes ($k_{\max} = l_{\max} = 32$ or 64) were sufficient to resolve the evolution. With 64^2 modes, there were roughly 20 grid points across the vortex diameter, and double that for 128^2 grid points. The model was advanced in time via a standard leapfrog scheme, with an Euler step applied periodically to stabilize the computational mode. Numerical stability was achieved by the use of an exponential cutoff filter with exponent four ([Canuto et al. 1988](#)). Potential vorticity was found to be better conserved and horizontal gradients better resolved under the action of such a filter than with the use of more traditional Laplacian ($\nu_2 \nabla^2 q_i$) or “biharmonic” damping ($\nu_4 \nabla^4 q_i$) schemes. Details are given in [LaCasce \(1996\)](#).

3. Scaling

Two parameters play a critical role hereafter and are obtained by scaling. Without a mean PV gradient at the surface, temporal evolution there is always nonlinear. But the β_2 restoring term in [\(2\)](#) permits wave-induced changes of the deep PV, so one may speak of the *relative* importance of advection at depth. Scaling [\(2\)](#) assuming velocity scales U_i , a length scale L , and a timescale proportional to the wave period, that is, $T \propto (\beta_2 L)^{-1}$, yields two parameters:

$$\Lambda \equiv \frac{F_2 \Delta U}{\beta_2}, \quad (5)$$

where $\Delta U \equiv |U_1 - U_2|$. The first indicates the importance of the advection of relative vorticity at depth and is a ratio of particle and wave speeds. Its inverse may be used to define an effective slope parameter, ϵ_2 . The second relates to the advection of “thickness,” or interfacial perturbations. When either term is larger than unity, there are closed contours of total PV at depth. If both are small, the slope contribution, $\beta_2 y$, dominates.

If the flow is barotropic, $\Lambda = 0$ because there is no interfacial displacement. Similarly, if the flow is surface trapped, $1/\epsilon_2 = 0$ and $\Lambda = F_2 U_1 / \beta_2$. This suggests that the importance of each parameter may be assessed separately (approximately) by considering initial flows that are purely barotropic or surface trapped. Thus, in [section \(5\)](#), I consider a barotropic vortex and, in [section \(6\)](#), one which is initially surface trapped.

4. Initial conditions

A vortex with a Gaussian streamfunction was chosen; that is,

$$\psi = A \exp\left(-\frac{r^2}{2r_0^2}\right) = -0.7 \exp\left(-\frac{r^2}{0.36}\right), \quad (6)$$

as shown in [Fig. 1](#). Such a choice is common in numerical studies (e.g., [McWilliams and Flierl 1979](#)) because the vortex azimuthal velocity decays exponentially in the far field, minimizing interactions with boundaries. The vortex is “isolated” in that the vanishing of the azimuthal velocity implies zero circulation; as such, a monopolar vortex is nested in a ring of oppositely signed vorticity (middle panel of [Fig. 1](#)). The Gaussian vortex is weakly barotropically unstable (e.g., [Carton 1989](#)), though this had little effect on the dynamics discussed below.

The barotropic vortex has the same profile in both layers. For the surface-trapped vortex, a vortex with $\psi_1(t_0)$ as above and $\psi_2(t_0) = 0$ was selected. There are other possible choices, such as a vortex that has zero perturbation PV initially at depth. The surface vortex was chosen so that there would be no topographic waves initially.

The vortex amplitude was such that the maximum azimuthal velocity (at $r = r_0$) was approximately 1.0. Only cyclonic vortices were considered, but as the QG equations are invariant under the change $\psi(y) \rightarrow -\psi(-y)$, the results for an anticyclone are exactly the same except for the reversal of the effective “north” and “south”; that is, if the cyclone moves toward shallower water, an equivalent anticyclone moves to deeper water.

5. A barotropic vortex

If there are two fluid layers and the vortex is initially barotropic ($U_1 = U_2 \equiv U$), there are two relevant parameters: the effective slope in [\(4\)](#), ϵ_2 , and the ratio of the scale of the vortex to the deformation scale, $Fr_0^2 \equiv (r_0/\lambda)^2$. The parameter space is seen in [Fig. 2](#). I will examine four extreme cases, denoted A–D. Cases A (large vortex) and B (small vortex) are over a weak slope, and C (small vortex) and D (large vortex) a strong slope. Intermediate slopes and vortex sizes are considered thereafter. The results are summarized schematically in [Fig. 2](#).

a. Case A: $r_0 = 2.5\lambda$, $\epsilon_2 = 0.02$


The evolution of a large vortex over a weak slope is seen in [Fig. 3](#). On the left are the surface PV and the total bottom PV ($q_2 + \beta_2 y$) at a late time, with the positions of the vortex center indicated every two time units. The centers or “PV centroids” are defined:¹

$$q_i \geq q_{\min} = 1.0 \quad (7)$$

where q_i is the perturbation PV in layer i . On the right are the “asymmetric streamfunction fields” at an early time. This field is the difference between the observed streamfunction and the initial streamfunction (scaled and translated to coincide with the former)² and is representative of the portion of the velocity field that propels the vortex (e.g., [Fiorini and Elsberry 1989](#)).

The vortex is moving barotropically. The upper and lower centroids are aligned, and upper-layer features are mirrored at depth. Moreover, the advecting asymmetric field is equally strong in both layers with a velocity at the vortex center that is parallel in both layers.


The vortex translation is self-induced, with a direction nearly cross-isobath but also weakly “westward.” The trajectory closely resembles that found for (isolated) barotropic vortices in the laboratory ([Carnevale et al. 1991](#)) as well as with single-layer vortices on the β plane (e.g., [Chan and Williams 1987](#)). The mechanism for self-induced motion on the β plane has been studied extensively, and is related to the interaction between the primary vortex and the perturbed background vorticity field. A cyclonic vortex advects fluid that lies initially to its east northward, and the latter acquires negative relative vorticity to conserve total vorticity. Likewise fluid to the west acquires positive relative vorticity as it is advected southward. The perturbed field thus is dipolar (the so-called β gyres) and propels the primary vortex that generated it.

In the topographic case, the perturbed vorticity field is necessarily bottom trapped, but the advecting gyres ([Fig. 3](#) ) are nearly barotropic because their scale exceeds the deformation scale. To see this, one inverts the (Fourier transformed) potential vorticities to obtain the streamfunctions:

$$\psi_1 = \frac{-(\kappa^2 + F_2)\hat{q}_1 - F_1\hat{q}_2}{\Delta} \quad (8)$$


$$\psi_2 = \frac{-F_2\hat{q}_1 - (\kappa^2 + F_1)\hat{q}_2}{\Delta}, \quad (9)$$

where $\Delta \equiv \kappa^2(\kappa^2 + F_1 + F_2)$, $\kappa^2 = \kappa^2 + l^2$ is the squared total wavenumber and $F_1 = F_2 = F$ by assumption. The “topographic gyres” are q_2 anomalies, so $q_1 = 0$. If the scale is large compared to the deformation radius, that is, $\kappa^2 \ll F$, then $\hat{\psi}_1 \approx \hat{\psi}_2$ and the streamfunction is nearly barotropic. If smaller, $\kappa^2 \gg F$, they are then bottom trapped, with $\hat{\psi}_1 \propto 1/\kappa^2$. The same reasoning applies to topographic waves.

As in the barotropic β -plane case, the barotropic vortex over a slope accelerates from rest to a quasi-steady translation speed.³ The translation speed is the same in the two layer, topographic case as it is in a one-layer fluid. Runs were made with purely barotropic and two-layer barotropic vortices, and the speeds of translation (found from least squares fits of the position of the upper vorticity centroid as a function of time) were compared; the results are shown in [Fig. 4](#) . The figure shows the magnitude of the translation velocity versus a scaled PV gradient in both cases.⁴ Not only are the velocities the same within error, but both velocities exhibit a square-root dependence on the mean PV gradient, that is, $u_t \propto \beta^{1/2}$, in the limit of a small gradient. [Smith \(1993\)](#) was apparently the first to recognize this dependence for barotropic vortices on the β plane.

Therefore, the case A evolution is consistent with that of a vortex in a purely barotropic environment. Next, a smaller vortex is considered.

b. Case B: $r_0 = 0.64\lambda$, $\epsilon_2 = 0.02$

The late PV fields and the asymmetric streamfunctions for a vortex smaller than deformation scale are seen in [Fig. 5](#) . Clearly this evolution is baroclinic. The initially barotropic vortex has separated into baroclinic vortices, each of which has a layer-trapped expression of potential vorticity. The erratic late motion moreover is also layer-trapped and is due to a dipolar interaction between the positive cores and the deformed outer rings of negative vorticity. The asymmetric streamfunctions

suggest that the surface and bottom halves of the vortex are moving at comparable speeds, but not in the same direction.

The exotic and rapid evolution in this case is the result of the so-called “twisting instability,” an azimuthal mode-one instability which affects subdeformation scale, barotropic-isolated vortices (Gent and McWilliams 1986; Flierl 1988). When such a vortex is submitted to a baroclinic perturbation, dipolar coupling between the inner core and outer ring of the vortex occurs in each layer, which tends to pull the vortex apart. The baroclinic perturbation in this case comes from the topographic gyres, which are now bottom-intensified and preferentially advecting the bottom vortex. Of course, the barotropic vortex over a slope is not a steady solution, and so one expects temporal development. The identification with the twisting instability is made because of the formation of baroclinic dipoles, which in turn causes an evolution more rapid than simple wave dispersion. The misaligned surface and bottom dipoles are evident in the asymmetric streamfunction in Fig. 5, and obscure the bottom-intensified topographic gyres.

The results of Gent and McWilliams (1986) suggest that the dividing line between stable and unstable vortices is sharp, so that vortices just larger than deformation scale are stable and those just smaller are not. This is borne out in Fig. 6, a plot of the distance between surface and bottom vorticity centroids. A vortex with $r_0 = 0.82\lambda$ separates (centroid distance increases monotonically) whereas one with $r_0 = 1.2\lambda$ does not. The intercenter distance oscillates for intermediate-scale vortices. Apparently the lower vortex, preferentially advected by the bottom-intensified topographic gyres, moves away from the upper, but then the upper *realigns* with the lower. Polvani (1991) studied the alignment of two potential vortices in different layers on the f plane, and found the phenomenon only occurs when the vortices are deformation scale or larger. This too is consistent with the present results. One notes again that phenomena such as this are transient over topography because the lower vortex is dispersing into topographic waves. The final state will be one without a vortex at depth, as discussed below.

Flierl (1988) points out that the outer ring of oppositely signed vorticity is required for instability. Consistent with this, additional runs with vortex with a Gaussian vorticity profile (no outer ring) produced nonseparating vortices (LaCasce 1996). Which vortex profile is more realistic is the subject of debate; however observations suggest that the ring azimuthal velocity field is compact (e.g., Olson et al. 1985).

The main point is that subdeformation-scale isolated vortices do not persist over topography. Moreover, the “flat bottom,” f -plane picture of vortex stability essentially applies. This is because dispersal of the lower portion of the vortex is very slow. The evolution when dispersal is rapid is quite different, as seen next.

c. Case C: $r_0 = 0.64\lambda$, $\epsilon_2 = 36$

Over a large slope, the evolution is quite different. The potential vorticity and streamfunction fields for such a case, with a vortex smaller than deformation scale and a large slope, are shown in Fig. 7. Two times are shown: soon *after* the initial instant and at a later time, to illustrate changes during and after the adjustment. The $t = 0$ fields are identical to those in cases A and B.

This evolution can be characterized as a rapid separation of the initial vortex into topographic waves and a surface-trapped vortex. The waves propagate rapidly off to the left—that is, with shallower water on their right, to where they are damped by a numerical “sponge layer,”⁵ and the vortex remains behind. The latter only has flow at the surface. In contrast to case B in which a vortex with surface-trapped PV was found, case C yields a vortex with a surface-trapped *streamfunction*. Furthermore, the surface PV does not appear to change during the evolution.

That the contours of total PV at depth are open suggests linearity in the bottom layer. This turns out to be true, and the final state is thus predictable. Inserting a wavelike solution $(\psi_1, \psi_2)\alpha \exp(ikx + ily - i\omega t)$ into the linearized versions of the PV equations (1)–(2) yields two solutions. The first is a propagating mode, the topographic Rossby waves, with

$$\omega = \frac{-\beta_2 k}{\kappa^2} \frac{\kappa^2 + F_1}{\kappa^2 + F_1 + F_2} \quad (10)$$

and

$$\psi_1 = \frac{F_1}{\kappa^2 + F_1} \psi_2. \quad (11)$$

The latter relation implies bottom intensification. These waves have zero surface potential vorticity; that is, $q_1 = 0$

identically. This solution is well known (e.g., [Rhines 1970](#); [Pedlosky 1987](#)); however, the equations have a second solution less frequently discussed: a stationary or “trivial” mode with $\omega = 0$. This mode carries the surface potential vorticity and has zero cross-isobath flow at depth ($\partial\psi_2/\partial x = 0$).

In an initial value calculation with a vortex, the entire lower-layer streamfunction and a portion of that at the surface disperse into waves, leaving the surface potential vorticity unchanged. Assuming no final flow at depth (i.e., no deep jets with $\mathbf{u}_2 = 0$), the remaining vortex properties are:

$$\psi_1(t_f) = \psi_1(t_0) - \frac{F_1}{\kappa^2 + F_1} \psi_2(t_0) = \frac{-\hat{q}_1}{\kappa^2 + F_1} \quad (12)$$

and

$$\hat{q}_2(t_f) = F_2 \psi_1(t_f) = \frac{-F_2 \hat{q}_1}{\kappa^2 + F_1}. \quad (13)$$

The upper-layer streamfunction is weaker than the initial streamfunction if the lower-layer streamfunction is initially of the same sign. For the barotropic vortex, the upper-layer streamfunction is weaker by a factor $\kappa^2/(\kappa^2 + F_1)$ so that vortices larger than deformation scale lose more than half the initial flow at the surface. The final lower-layer PV is nonzero, and is due only to the interfacial stretching caused by the upper vortex.

Interestingly, the final vortex does not depend at all on the initial lower-layer PV, only on q_1 . Thus an initially barotropic vortex and one that initially has no flow at depth will yield the same final vortex (identical to the latter vortex) if the two have the same surface PV. This does not, of course, imply an independence of ψ_2 because ψ_2 in part determines q_1 , and the loss of the ψ_1 to waves is directly proportional to ψ_2 .

Cross sections of the surface streamfunction from the numerical calculation and the linear prediction are shown in [Fig. 8](#). The amplitude and scale agree quite well, although the predicted amplitude is somewhat less than observed, and the predicted azimuthal velocity, $\partial\psi_1/\partial r$ changes sign, unlike with the observed vortex. Nevertheless, the differences are small and within the realm of possible numerical effects. Surprisingly, a linear solution succeeds despite that the surface flow is strongly nonlinear.

The question of how much topographic wave energy is generated by a ring impacting on the slope has been considered by [Louis and Smith \(1982\)](#) and [Shaw and Divakar \(1991\)](#). Given the linear construction above, it is straightforward to derive the wave energy, if one knows the strength of the initial deep flow ([LaCasce 1996](#)). The amount of energy is found to equal that lost by the vortex, as one might expect by conservation of total energy.

d. Case D: $r_0 = 2.5\lambda$, $\epsilon_2 = 36$

A barotropic vortex larger than deformation scale is expected to radiate waves that are significantly barotropic, leaving a much weakened surface vortex. The fields for a vortex with $r_0 = 2.5\lambda$ ([Fig. 9](#)) show this to be true. The waves are indeed nearly barotropic, as seen in the streamfunction plots at $t = 0.1$, and the final surface vortex greatly weakened ($t = 2.0$).

One also finds that the surface PV again evolves only slightly during wave radiation. This suggests that the evolution is likely to be linear in the sense of the previous section. The final streamfunction and that predicted by linear theory are shown in [Fig. \(10\)](#). The amplitude and size of the vortex are predicted well. In fact, the primary difference between this case and case C is the degree to which the surface vortex is weakened by radiation; both cases yield a surface-trapped vortex and topographic waves. This is in strong contrast to the weak slope case in which there was a marked change in the *qualitative* behavior at the deformation radius.

e. Intermediate slopes

Initially barotropic vortices over extremely weak and strong slopes have been discussed. In this section, the evolution over intermediate slopes is considered. Additional numerical runs with the $r_0 = 0.64\lambda$ and the $r_0 = 2.5\lambda$ vortices were made;

representative PV plots at late times are shown in [Figs. 11–12](#), from which one may infer the transition from small to large slopes.

In general, the behavior over “medium” slopes is intermediate between the two extremes. One finds that increasing the grade increases the rate of dispersion of the deep vortex. For the $r_0 = 0.64\lambda$ vortex, the surface portion remains intact in all cases. The difference is the extent to which it is perturbed by the deep vortex; the faster the dispersion, the weaker the perturbation at the surface. There is little weakening of the surface streamfunction by radiating waves because the waves are strongly bottom intensified.

In contrast, the larger vortex ([Fig. 12](#)) has strong coupling between the upper and lower portions. Thus the more rapid dispersion of the deep vortex at $\epsilon_2 = 0.18$ is accompanied by severe distortion at the surface. In the case $\epsilon_2 = 1.8$, this distortion is strong enough to cause fission at the surface. The latter is of some interest because this is the only region of parameter space where the surface vortex is actually “destroyed.” Fission is found to occur only when the initial deep flow is strong, and the slope is order unity; that is, $\epsilon_2 = O(1)$. This too may be argued by scaling. Assume that the deep flow is wavelike. Decomposing the surface streamfunction into wave and vortex portions; that is, $\psi_1 = \psi_{1w} + \psi_{1v}$ and noting that the waves have no PV at the surface, [\(1\)](#) can be rewritten:

$$\frac{\partial}{\partial t} q_1 + J(\psi_{1v}, q_1) + J(\psi_{1w}, q_1) = 0. \quad (14)$$

The second term represents vortex self-induced advective changes to PV, and is zero if the streamlines and isolines of q_1 are parallel, as with the initial axisymmetric vortex. The third term represents wave-induced changes to PV. If the waves are to dominate the evolution of the surface PV, term three must be comparable to or greater than term two and must be comparable to term one. Scaling [\(14\)](#) assuming a wave timescale and using the relation $\hat{\psi}_{1w} = F_1 \hat{\psi}_{2w}/(\kappa^2 + F_1)$ yields the following simultaneous conditions for wave-induced changes:

$$\frac{U_{1w}}{U_{1v}} \approx \left(\frac{2F_1 r_0^2}{1 + F_1 r_0^2} \right) \frac{U_2}{U_1} > 1 \quad (15)$$

and

$$\frac{U_{1w}}{\beta_2 r_0^2} \approx \frac{F_1 r_0^2}{1 + F_1 r_0^2} \frac{U_2}{\beta_2 r_0^2} = \frac{F_1 r_0^2}{\epsilon_2 (1 + F_1 r_0^2)} \approx 1. \quad (16)$$

The two conditions taken together require that 1) the vortex be larger than deformation scale, 2) the deep flow be sufficiently intense, and 3) that the slope be $\epsilon_2 = O(1)$. The case D vortex met the first two criteria, but the slope was too great. The third vortex in [Fig. 12](#) meets all three criteria. In this case, the third term in [\(14\)](#) is much larger than the second, and the equation is formally the same as that for the advection of a passive tracer. Thus the waves shear the surface vortex apart. My choice of an initially barotropic vortex yields an intense deep flow; more realistic oceanic vortices have weaker flow at depth, which makes such shearing less likely.

f. Summary

The barotropic vortex results are summarized schematically in [Fig. 2](#). The vortex remains barotropic only when it is larger than deformation scale and the slope is very weak. If the slope is such that $\epsilon_2 \equiv f(\partial_y H) r_0^2 / (H_2 U_2) \geq 1$, the lower portion disperses into topographic waves, leaving a weakened and stationary surface vortex. If the waves are strong enough at the surface and of a period comparable to the advective timescale of the surface vortex, the waves can disturb and even shear out that vortex (the gray region of the figure); if the wave timescale is much shorter or the waves weak, the surface remains coherent. Subdeformation scale vortices were always found to become baroclinic, evolving to either layer-trapped potential vortices (weak slope) or a surface vortex and waves (strong slope).

Weaker deep flow favors dispersion because a small U_2 means a larger effective slope, ϵ_2 . It also suggests that wave-induced disruption of the surface vortex will be less likely because the wave strength at the surface will be weaker. In other words, the gray region of [Fig. 2](#) will be less prominent.

6. A surface vortex

The relevance of the parameter $\Lambda = F\Delta U/\beta_2$ is now considered. As this parameter relates the importance of stretching to a mean PV gradient (the slope), one imagines that it might be relevant to the release of available potential energy (APE). Indeed, the condition for the baroclinic instability of a zonal flow on the β plane involves a similar parameter (e.g., [Pedlosky 1987](#)). The following examples suggest that Λ is indeed a measure of instability.


The stability of a baroclinic vortex over a flat bottom has been studied previously (e.g., [Ikeda 1981](#); [Flierl 1988](#); [Helfrich and Send 1988](#)). In general, vortices larger than deformation scale and not too barotropic are baroclinically unstable, with the most unstable azimuthal mode number increasing with vortex scale. In the finite-amplitude state, unstable vortices tend to break into deformation-scale baroclinic dipoles ([Ikeda 1981](#); [Helfrich and Send 1988](#)).



The influence of topography has received less attention. [Hart \(1975\)](#) considered the linear stability of a surface-trapped, two-layer flow in a circular basin, in effect a vortex with “walls,” over a linear slope. He found that a weak slope destabilizes small-scale disturbances but that steep slopes damp unstable growth rates, postulating that the vortex would become stable in the limit of a very large slope since fluid parcels would be constrained to move along isobaths.

In the following I consider the evolution of a weakly perturbed surface Gaussian vortex over linear slopes. As mentioned before, I use the surface streamfunction of the barotropic vortex of the last section so that ψ_1 is the Gaussian given in [\(6\)](#) and $\psi_2 = 0$. A perturbation of azimuthal mode 2 was added to the resulting surface relative vorticity, at 15% of the vortex amplitude, to hasten unstable growth. Again, the layer depths are taken to be equal. Four examples are presented first to illustrate what can happen as vortex size and slope are varied. Then the effect of the slope on stability is discussed in broader terms.


It is useful to nondimensionalize the slope; however, ϵ_2 as defined in [section 3](#) is initially infinite. One might use Λ , but it turns out that a better approach is to use the surface velocity to define $\epsilon_1 \equiv \beta_2 r_0^2 / U_1$. Such a definition yields continuity with the previous section because ϵ_1 for the surface vortex is the same as ϵ_2 for the barotropic vortex initially. In addition, this choice permits one to see how Λ is, in fact, the controlling parameter.


The four examples are as follows: a large vortex ($r_0 = 2.5\lambda$)⁶ over a flat bottom ($\epsilon_1 = 0$), the same vortex over an intermediate slope ($\epsilon_1 = 3.6$), and over a strong slope ($\epsilon_1 = 18$). The fourth case is with a larger vortex ($r_0 = 4.2\lambda$) over the same nondimensional slope, ($\epsilon_1 = 18$). The slope parameter was determined using the maximum surface velocity, or $U_1(r_0)$. The corresponding values of Λ for these cases are ∞ , 1.8, 0.36, and 1.0, again using the maximum surface velocity for scaling.

Representative potential vorticity fields ($t = 15$) for each case are shown in [Figs. 13–14](#) . In the flat bottom case, the large surface-trapped vortex splits into a small, stationary surface vortex and two deformation-scale baroclinic dipoles. The latter move away from one another, one to the left and the other to the right. Each dipole consists of a surface cyclonic potential vortex and a bottom anticyclonic vortex displaced horizontally from it. The evolution is exactly as that described by [Ikeda \(1981\)](#) and [Helfrich and Send \(1988\)](#), where the reader may find additional details. Such baroclinic dipoles are often called “hetons” (e.g., [Hogg and Stommel 1985](#)) because they can transport heat (thickness) anomalies laterally.

Over a weak slope ($\epsilon_1 < 1$, not shown), the short-term evolution is qualitatively the same, with the vortex breaking into baroclinic dipoles which translate away from one another. Over longer periods of time, the deep vortices tend to disperse at a rate that depends on the strength of the slope. This obviously retards translation of the final baroclinic dipoles. Over larger slopes, translation ceases earlier, and when ($\epsilon_1 = O(1)$) dispersal happens at the same time as the instability. Such a case is seen in the lower panels of [Fig. 13](#) . The upper vortex has split into smaller vortices, the outer ring of negative vorticity has been dispersed into small-scale anomalies, and the deep flow is devoid of coherent vortices. As a result, no dipole formation occurs, either with anomalies at the surface (e.g., [section 5b](#)) or bottom (e.g., upper panels of [Fig. 13](#) ) , so the positive surface vortices are unable to move away from the site of instability.

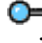
Previously it was found that the deep portion of an initially barotropic vortex disperses rapidly at depth if $\epsilon_2 \geq 1$. As noted, $\epsilon_2 = \infty$ initially, hindering an a priori assessment of whether dispersal will occur. However, if the vortex is approximately deformation scale, one expects that $U_2(t_p) \approx U_1(t_0)$ ⁷, so that $\epsilon_2(t_p) \approx \epsilon_1(t_0)$, suggesting that dispersal ought to occur when $\epsilon_1 \geq 1$.

In the case of a larger slope ($\epsilon_1 = 18$), the vortex appears to be stable, seen in [Fig. 14](#) ; the final vortex resembles the initial vortex and little potential energy has been lost. A close examination of the deep streamfunction reveals that there is some wave radiation while the surface vortex relaxes to an axisymmetric state, but that the waves are transient. The final vortex is larger than deformation scale, and the motion in the two layers is decoupled. Thus, as conjectured by [Hart \(1975\)](#), instability may be defeated by a large enough slope.

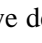
The final example illustrates that a large value of ϵ_1 , or the slope β_2 for that matter, does not necessarily imply stability. In the lower frames of [Fig. 14](#)  we see that a somewhat larger vortex ($r_0 = 4.2\lambda$) becomes unstable over the same slope.


This is not to say that the evolution is the same as in the flat bottom case. Here, disturbances appear to grow along the edge of the vortex and couple to topographic waves that radiate away. The disturbances then apparently die down. APE is lost gradually, and the surface vortex does not break into smaller vortices. At late times (not shown), the surface PV is found to separate into smaller pieces, simply because the surface vortex is too weak to remain intact. The main point is that instability in the case $\epsilon_1 > 1$ is qualitatively distinct from the explosive separation over the flat bottom, and is characterized by radiation of topographic waves.⁸

Instability in the presence of a strong slope may be rationalized as follows (J. Pedlosky 1996, personal communication). It is known that a nonzonal current cannot be completely stabilized by the β effect ([Pedlosky 1987](#)) because disturbances with particle motion parallel to latitude lines are not stabilized by β . A vortex has flow both parallel and perpendicular to the isobaths, so if large enough, one expects that the slope will be unable to stabilize small disturbances in regions where the vortex flow is not parallel to the slope. Nevertheless, as seen next, one can always find a *steeper* slope that will stabilize a vortex with a fixed radius.

Time series of APE summarize the differences in instability between various runs ([Fig. 15](#) ). In the top panel is the APE for a vortex with $r_0 = 2.5\lambda$. When the bottom is flat ($\epsilon_1 = 0$), the potential energy decreases rapidly. It decreases equally fast in the $\epsilon_1 = 3.6$ case, showing that the topography has not retarded the loss of APE despite forcing the dispersal of deep vortices. Increasing the slope further does inhibit the conversion of PE, and the vortex is apparently stable over the largest slope.

In the lower panel, the slope is fixed ($\epsilon_1 = 3.6$) but the vortex size is varied. One sees that APE is lost if the vortex is large enough. The smallest vortices are stabilized by the slope, but larger vortices are unstable. Note there is a qualitative difference with the flat bottom case in that APE tends to decay more slowly. Moreover, one finds oscillations in time. The frequency of these oscillations is proportional to β_2 , suggesting they are related to the topographic waves.

To see how stability varies over a broader range of parameters, a large number of experiments were made, and the results tabulated as follows. Each run employed a weakly perturbed surface Gaussian vortex and was run to a fixed time ($t = 20$). The APE was calculated and fit in a least squares sense to a cubic function (to remove the aforementioned oscillations; an example of such a fit is shown in the lower panel of [Fig. 15](#) ). From this curve, the relative decay of APE over the time period; that is, PE_{20}/PE_0 , was calculated. This ratio was used as a marker for the degree of instability in the run.

The results are shown in [Fig. 16](#)  as a function of $Fr_0^2 = (r_0/\lambda)^2$ and the nondimensional slope, $\epsilon_1 = \beta_2 r_0^2 / U_1$. The upper and lower panels show the same curves, but the upper is against the logarithm of the slope. The experiments in which the relative loss of APE exceeded 5% were deemed “unstable,” and those with less values were “stable.” Of course, the method depends on the length of integration and choice of the cutoff value. Nevertheless, the curves obtained with other choices of cutoff number fall very close to the $PE_{20}/PE_0 = 0.95$ curve. The latter is taken as a numerical proxy for the actual neutral stability curve.

As suggested by [Hart \(1975\)](#) a weak slope weakly destabilizes the vortex, as seen by the slight dip in the curve near $\epsilon_1 = 0.1$ in the top panel. The more obvious effect is that larger slopes ($\epsilon_1 > 1$) stabilize the surface vortex. The curve that separates stable and unstable vortices is linear when $\epsilon_1 > 1$, as seen in the lower panel, and has a slope of 0.45 ± 0.15 . The vortex is thus stable when $Fr_0^2 < 0.45\beta_2 r_0^2 / U_1$, or equivalently $\Lambda < 0.45$. Thus Λ emerges as the important parameter in terms of the stability of the surface-trapped vortex.

Larger values of ϵ_1 could not be tested with this model due to problems with fast reentrant waves. A more complete specification of the Λ dependence likely will come with a proper analytical stability solution. Also note that the surface velocity scale was chosen so that $U_1 = 1$, the value of the maximum azimuthal velocity. If I had chosen $U_1 = 0.45$,

approximately the velocity at the e -folding radius, the slope of the curve would have been one. In other words, the condition for stability would be $\Lambda < 1$ if Λ is defined in terms of a “mean” surface velocity.

a. Summary

The baroclinic stability of a Gaussian surface vortex has been considered. By varying vortex sizes and an effective slope defined in terms of the surface velocity (ϵ_1), a dependence on $\Lambda \equiv FU_1/\beta_2$, where U_1 is the maximum, was deduced.

When this parameter is less than about one-half, the surface vortex is stable despite being larger than deformation scale. In addition, if the slope is large enough so that $\epsilon_1 > 1$, the instability is predominantly a radiating one characterized by a steady leakage of topographic waves. In such a case, the formation of baroclinic dipoles or “hetons” is defeated.

Note the stability criteria is roughly equivalent to that which guarantees open contours of deep PV; that is, the slope contribution to PV overwhelms that due to interfacial stretching. The parameter Λ depends on slope and stratification, so one can always find a slope to stabilize a given vortex, but it is also possible to find an unstable vortex for any given slope.

7. Discussion

A vortex over topography may behave much differently than one over a flat bottom. Topography favors *dispersal* of deep flows, and thus surface-trapped vortices over barotropic ones. Second, topography can *stabilize* a surface vortex, permitting the existence of baroclinic vortices larger than deformation scale. Over a slope, these two effects are gauged simply by two parameters, $\epsilon_2 \equiv \beta_2 r_0^2 / U_2$ (dispersal) and $\Lambda \equiv F_2 U_1 / \beta_2$ (stability), each obtained by scaling. Both parameters are measures of the effective severity of the slope for a given vortex. Significantly, the effective slope is a function not only of the topographic grade but also stratification and the length and velocity scales of the vortex.

The present findings suggest self-induced translation of vortices over topography (e.g., [Carnevale et al. 1991](#)) occurs only when the vortex is larger than deformation scale, significantly barotropic, and the slope very weak ($\epsilon_2 \ll 1$). If $\epsilon_2 \geq 1$, the deep flow is dispersed and there is no topographic translation. Thus, the suggestion (e.g., [Smith and O'Brien 1983](#); [Carnevale et al. 1991](#); [Grimshaw et al. 1994b](#)) that the direction of translation on the β plane and over a slope will be relative to a weighted mean “northwest” is incorrect over strong slopes. The lack of topographic translation may help explain why warm core rings impact on the continental slope and move to the topographic west, whereas the Loop Current eddies in the Gulf of Mexico drift to the topographic east after impact. Both vortices may simply be interacting with the local mean flow subsequent to topographic wave radiation. If so, the apparent topographic “steering” would be related to the mean flow, which presumably follows the isobaths rather than a vortex/topography interaction. Over weak slopes the “mean northwest” assertion applies, but again “weak” implies a slight topographic grade and intense deep flow.

The present results may also explain the discrepancy between the laboratory results of [Mory et al. \(1987\)](#) and [Whitehead et al. \(1990\)](#). Both studies examined the motion of bottom-trapped vortices formed by convection over a shelf. In the Mory et al. case the vortex migrated slowly to the northwest across the slope, whereas in the Whitehead et al. case the vortex had no apparent deep circulation and drifted along the isobaths. Given the present results, one suspects that the former vortex was nearly barotropic (case A), whereas the deep circulation of the latter was lost to topographic wave radiation (case D). Scaling from the published parameters suggests that ϵ_2 was perhaps three times greater in the Whitehead et al. case ([LaCasce 1996](#)).

Dispersal of the deep flow when $\epsilon_2 \geq 1$ yields a vortex that is “compensated,” or surface-trapped. Compensation was noted in all the numerical runs in the study of an Agulhas eddy traversing a deep ridge by [Kamenkovich et al. \(1996\)](#).

Deep dispersal can alter the finite amplitude state of baroclinic instability. The preferred state over moderate to large slopes ($\epsilon_2 \geq 1$) is one with surface vortices and topographic waves, rather than baroclinic dipoles or “hetons” ([Hogg and Stommel 1985](#)). As such, topography may significantly alter the processes of deep convection from the surface (e.g., [Maxworthy and Narimousa 1994](#)) or the formation of convective plumes over ridges (e.g., [Speer and Marshall 1995](#)).

The present results predict a weakening of the surface portion of a ring impacting on a slope if that ring has deep flow. As noted earlier, there is some observational evidence for such an effect. [Vidal et al. \(1994\)](#) noted that a Loop Current eddy was weakened by roughly 30% upon hitting the continental slope, and [Cheney and Richardson \(1976\)](#) similarly found a marked decrease in the strength of a cold core ring passing over the Blake Escarpment. Interestingly, if one knows the extent to which the surface vortex is weakened, it is possible to estimate the strength of the initial deep flow given the results of [section 5c](#). A 30% decrease, as in the Vidal et al. case, implies that the deep flow was roughly half as strong as the surface flow, and so significantly barotropic. If so, this may explain why such a vortex, substantially larger than the deformation radius, was baroclinically stable prior to impacting the slope.

The “destruction” of vortices over steep topography, seen in barotropic simulations such as those of [Grimshaw et al. \(1994a\)](#), does not occur in these two-layer examples. This is a consequence of baroclinicity and the vertical structure of topographic waves. So long as the vortex is not expressible as a sum of topographic wave modes, which is the case if it is surface intensified or barotropic, one always expects a surface vortex to be “left over” after wave radiation. [Richardson et al. \(1989\)](#) observed a meddy disperse near very steep topography and noted that subsequent surveys were unable to locate the vortex remains. The present results suggest that a vortex was left behind, though it was likely smaller and harder to observe.

Given published dimensions for oceanic rings and the principal topographic features with which they interact, one can estimate these parameters. The following examples (see [Table 1](#)) are drawn from estimates of ring and slope parameters from warm core ring 82B over the continental slope off the east coast of the United States (WCR: [Joyce, 1984](#); [Olson et al. 1985](#)), an Agulhas eddy over the Walvis Ridge (AE: [Clement and Gordon 1995](#); [Kamenkovich et al. 1996](#)), a Loop Current eddy impinging on the continental slope in the western Gulf of Mexico (LCE: [Cooper et al. 1990](#); [Vidal et al. 1994](#)), and a North Brazil Current retroflection eddy off the coast of Brazil (NBRE: [Richardson et al. 1994](#); [Flagg et al. 1986](#)). (One may rewrite $\Lambda = F_2 U_1 / \beta_2$ as $\Lambda = f U_1 / (g' \partial_y H)$, and the second expression is evaluated above.) The velocity scales are only representative values, and the deep velocity is typically not well known.⁹ Similarly, the surface velocities tend to vary substantially; Loop Current eddies exhibit peak velocities near 2.0 m s^{-1} after formation ([Cooper et al. 1990](#)), but they are perhaps half that upon reaching the western Gulf of Mexico. The slopes vary too substantially, and the values here are only indicative.

The suggestion from the scalings is that these vortices all fall into the “strong slope” category so that one would expect rapid dispersal of deep flow and baroclinic stability over the slope. Moreover, the weakness of the deep flow and large size of ϵ_2 suggest that vortex deformation by wave radiation ([section 5e](#)) is unlikely. Observations seem to support these conclusions. Warm core rings tend to move onto the continental slope and exist for many months without breaking into smaller vortices; they also do not traverse the slope and move onto the shelf. Loop Current eddies and Brazil retroflection eddies ([Richardson et al. 1994](#)) apparently behave similarly.

The focus of the present work has been the evolution of two specific initial vortices (barotropic and surface trapped). These were chosen, as noted earlier, so that the effects of the two parameters, ϵ_2 and Λ , could be weighed separately. But of course, other profiles are possible, and in such cases both parameters may be relevant. Consider an arbitrary vortex, perhaps stronger at the surface. As it encounters a slope, the value of ϵ_2 would suggest the degree of deep dispersion, and whether, for instance, one would expect topographic migration, surface vortex weakening or even surface vortex shearing. Given that information, one might then ask whether the final vortex, which will be surface trapped over stronger slopes, is also baroclinically stable. This requires a knowledge of the (weakened) vortex size and of Λ , which in principle is predictable (e.g., [section 5c](#)). The point is that the separate effects, illustrated by the present chosen initial vortices, are likely to be relevant to more general profiles.

It should also be emphasized that a knowledge of ϵ_2 and Λ permits an assessment of the qualitative aspects of the evolutions, quantitative aspects of course will depend on other quantities (such as the ratio F_1/F_2). For example, the vortex scale relative to the surface deformation radius is important in terms of the degree of surface vortex weakening following topographic wave radiation or the rate of unstable growth. But it is nevertheless useful to categorize the various types of response, which follow from knowledge of ϵ_2 and Λ .

The present work excludes the planetary β effect. With β restored, a monopolar vortex at the surface is no longer a stationary solution of the equations. When the slope is strong, there are now two propagating waves: the same topographic wave and a slow surface-trapped planetary wave ([LaCasce 1996](#)), similar to the continuously stratified case where one finds the bottom-trapped wave and an infinite number of surface waves, each with a node at the bottom ([Rhines 1970](#)). The surface wave would cause a weak dispersal of the surface vortex in cases C and D, perhaps allowing it to move meridionally despite being compensated, as seen in [Kamenkovich et al. \(1996\)](#). However, motion is not guaranteed; their nearly barotropic vortex stalled over the ridge. Apparently, the slope can disable vortex translation by inhibiting formation of the planetary β gyres [[Y. G. Morel \(1996\)](#), personal communication; [Thierry and Morel \(1997\)](#)].

The present results assume quasigeostrophy, which implies weak slopes. Stronger slopes can introduce additional effects. If the topography penetrates the upper layer, for example, the structure of the final surface vortex will clearly be different. Moreover, the presence of an adjacent shelf opens the possibility of interactions with fluid stripped off the shelf (e.g., [Wang 1992](#)). A full realization with such complexities obviously requires more sophisticated models. However, the general tendencies of deep dispersion and slope-induced changes to stability will likely be relevant.

Oceanic observations suggest that rings and such eddies are surface intensified. It is important to consider further to what

extent topography is responsible for such a state.

Acknowledgments

I am grateful to Ken Brink for numerous readings and many interesting conversations. I am also indebted to committee members Dave Chapman, Glenn Flierl, Steve Lentz, and Joe Pedlosky for suggestions that greatly improved the work. Glenn Flierl provided the two-layer quasigeostrophic code, and the numerical filter was implemented by Audrey Rogerson. Funding for this work was provided by Grants N00014-92-J-1643 and N00014-92-J-1528 from the U.S. Office of Naval Research (Coastal Dynamics code).

REFERENCES

- Adem, J., 1956: A series solution for the barotropic vorticity equation and its application in the study of atmospheric vortices. *Tellus*, **8**, 364–372..
- Canuto, C., M. Y. Hussaini, A. Quarteroni, and T. A. Zang, 1988: *Spectral Methods in Fluid Mechanics*. Springer-Verlag, 567 pp..
- Carnevale, G. F., R. C. Kloosterziel, and G. J. F. van Heijst, 1991: Propagation of barotropic vortices over topography in a rotating tank. *J. Fluid Mech.*, **233**, 119–140..
- Carton, X., 1989: Barotropic and baroclinic instabilities of axisymmetric vortices in a QG model. *Mesoscale/Synoptic Coherent Structures in Geophysical Turbulence*. J. C. J. Nihoul and B. M. Jamart, Eds., Elsevier, 225–244..
- Chan, J. C.-L., and R. T. Williams, 1987: Analytical and numerical studies of the beta-effect in tropical cyclone motion. Part I: Zero mean flow. *J. Atmos. Sci.*, **44**, 1257–1265.. [Find this article online](#)
- Cheney, R. E., and P. L. Richardson, 1976: Observed decay of a cyclonic Gulf Stream ring. *Deep-Sea Res.*, **23**, 143–155..
- Clement, A. C., and A. L. Gordon, 1995: The absolute velocity field structure of Agulhas eddies and the Benguela Current. *J. Geophys. Res.*, **100**, 22 591–22 601..
- Cooper, C., G. Z. Forristall, and T. M. Joyce, 1990: Velocity and hydrographic structure of two Gulf of Mexico warm core rings. *J. Geophys. Res.*, **95**, 1663–1679..
- Faller, A. J., and W. S. von Arx, 1955: On the variation of the Coriolis parameter and its simulation in models of ocean circulation. Woods Hole Oceanographic Institution Tech. Rep., WHOI-55-13, 16 pp. [Available from Woods Hole Oceanographic Institution, Woods Hole, MA 02543.].
- Fiorini, M., and R. L. Elsberry, 1989: Some aspects of vortex structure related to tropical cyclone motion. *J. Atmos. Sci.*, **46**, 975–990.. [Find this article online](#)
- Flagg, C. N., R. L. Gordon, and S. McDowell, 1986: Hydrographic and current observations on the continental slope and shelf of the western equatorial Atlantic. *J. Phys. Oceanogr.*, **16**, 1412–1429..
- Flierl, G. R., 1988: On the instability of geostrophic vortices. *J. Fluid Mech.*, **197**, 349–388..
- , 1994: Semicohherent oceanic features. *Chaos*, **4**, 355–367..
- Gent, P. R., and J. C. McWilliams, 1986: The instability of barotropic circular vortices. *Geophys. Astrophys. Fluid Dyn.*, **35**, 209–233..
- Grimshaw, R., D. Broutman, X. He, and P. Sun, 1994a: Analytical and numerical study of a barotropic eddy on a topographic slope. *J. Phys. Oceanogr.*, **24**, 1587–1607..
- , Y. Tang, and D. Broutman, 1994b: The effect of vortex stretching on the evolution of barotropic eddies over a topographic slope. *Geophys. Astrophys. Fluid Dyn.*, **76**, 43–71..
- Hart, J. E., 1975: Baroclinic instability over a slope. Part I: Linear theory. *J. Phys. Oceanogr.*, **5**, 625–633..
- Helfrich, K. R., and U. Send, 1988: Finite-amplitude evolution of two-layer geostrophic vortices. *J. Fluid Mech.*, **197**, 331–348..
- Hogg, N. G., and H. M. Stommel, 1985: The heton, an elementary interaction between discrete baroclinic geostrophic vortices, and its implications concerning eddy heat-flow. *Proc. Roy. Soc. London A*, **37**, 1–20..

- Ikeda, M., 1981: Instability and splitting of mesoscale rings using a two-layer quasi-geostrophic model on an f -plane. *J. Phys. Oceanogr.*, **11**, 987–998..
- Joyce, T. M., 1984: Velocity and hydrographic structure of a Gulf Stream warm-core ring. *J. Phys. Oceanogr.*, **14**, 936–947..
- Kamenkovich, I. V., and J. Pedlosky, 1996: Radiating instability of nonzonal ocean currents. *J. Phys. Oceanogr.*, **26**, 622–643..
- , Y. P. Leonov, D. A. Nechaev, D. A. Byrne, and A. L. Gordon, 1996: On the influence of bottom topography on the Agulhas Eddy. *J. Phys. Oceanogr.*, **26**, 892–912..
- LaCasce, J. H., 1996: Baroclinic vortices over a sloping bottom. Ph.D. thesis, M.I.T./W.H.O.I. Joint Program in Oceanography, 216 pp. [Available from Joe LaCasce, Woods Hole Oceanographic Institution, M.S. 29, Woods Hole, MA 02543.].
- Louis, J. P., and P. C. Smith, 1982: The development of the barotropic radiation field of an eddy over a slope. *J. Phys. Oceanogr.*, **12**, 56–73..
- Maxworthy, T., and S. Narimousa, 1994: Unsteady, turbulent convection into a homogeneous, rotating fluid, with oceanographic applications. *J. Phys. Oceanogr.*, **24**, 865–887..
- McWilliams, J. C., and G. R. Flierl, 1979: On the evolution of isolated, nonlinear vortices. *J. Phys. Oceanogr.*, **9**, 1155–1182..
- Mied, R., and G. J. Lindemann, 1979: The propagation and evolution of cyclonic Gulf Stream rings. *J. Phys. Oceanogr.*, **9**, 1183–1206..
- Mory, M., M. E. Stern, and R. W. Griffiths, 1987: Coherent baroclinic eddies on a sloping bottom. *J. Fluid Mech.*, **183**, 45–62..
- Olson, D. B., R. Schmitt, M. Kennelly, and T. Joyce, 1985: Two-layer diagnostic model of the long-term physical evolution of warm-core ring 82 B. *J. Geophys. Res.*, **90**, 8813–8822..
- Pedlosky, J., 1987: *Geophysical Fluid Dynamics*. Springer-Verlag, 710 pp..
- Polvani, L. M., 1991: Two-layer geostrophic vortex dynamics. Part 2. Alignment and two-layer V-states. *J. Fluid Mech.*, **225**, 241–270..
- Reznik, G. M., and W. K. Dewar, 1994: An analytical theory of distributed axisymmetric barotropic vortices on the beta-plane. *J. Fluid Mech.*, **269**, 301–321..
- Rhines, P. B., 1970: Edge-, bottom- and Rossby waves in a rotating, stratified fluid. *Geophys. Fluid Dyn.*, **1**, 273–302..
- Richardson, P. L., D. Walsh, L. Armi, M. Schroder, and J. F. Price, 1989: Tracking three meddies with SOFAR floats. *J. Phys. Oceanogr.*, **19**, 371–383..
- , G. E. Hufford, and R. Limeburner, 1994: North Brazil Current retroflection eddies. *J. Geophys. Res.*, **99**, 5081–5093..
- Sakamoto, T., and T. Yamagata, 1997: Evolution of baroclinic planetary eddies over localized bottom topography in terms of JEBAR. *Geophys. Astrophys. Fluid Dyn.*, **84**, 1–27..
- Shaw, P. T., and S. Divakar, 1991: Generation of topographic waves over the continental margin. *J. Phys. Oceanogr.*, **21**, 1032–1042..
- Smith, D. C., IV, and J. J. O'Brien, 1983: The interaction of a two-layer isolated mesoscale eddy with bottom topography. *J. Phys. Oceanogr.*, **13**, 1681–1697..
- Smith, R. B., 1993: A hurricane beta-drift law. *J. Atmos. Sci.*, **50**, 3213–3215.. [Find this article online](#)
- Speer, K. G., and J. Marshall, 1995: The growth of convective plumes at seafloor hot springs. *J. Mar. Res.*, **53**, 1025–1057..
- Thierry, V., and Y. G. Morel, 1999: Influence of a strong bottom slope on the evolution of a surface intensified vortex. *J. Phys. Oceanogr.*, in press..
- van Ballegooyen, R. C., M. L. Grundlingh, and D. Lutjeharms, 1994: Eddy fluxes of heat and salt from the southwest Indian Ocean into the southeast Atlantic Ocean: A case study. *J. Geophys. Res.*, **99**, 14 053–14 070..
- Vidal, V. M. V., F. V. Vidal, and J. M. Perez-Molero, 1994: Collision of a loop current anticyclone ring against the continental shelf–slope of the western Gulf of Mexico. *J. Geophys. Res.*, **99**, 2155–2172..
- Wang, X., 1992: Interaction of an eddy with a continental slope. Ph.D. thesis, M.I.T./W.H.O.I. Joint Program in Oceanography, 216 pp..
- Whitehead, J. A., M. E. Stern, G. R. Flierl, and B. A. Klinger, 1990: Experimental observations of baroclinic eddies on a sloping bottom. *J. Geophys. Res.*, **95**, 9585–9610..

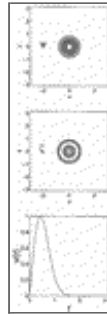
Tables

Table 1. Characteristics for oceanic rings for selected regions.

Ring	U_0	U_1	ϵ_0	H_0	ρ'	$f(\times 10^{-3})$	βH	ϵ_1	λ
WCR	1.0	0.05	50000	2000	0.01	9.4	0.025	60	0.4
US	1.0	0.1	100000	4000	0.04	9.4	0.0125	30	0.2
LCI	1.0	0.1	100000	3000	0.025	6.2	0.01	30	0.4
NBR	0.8	??	125000	3000	0.03	2.5	0.02	??	0.033

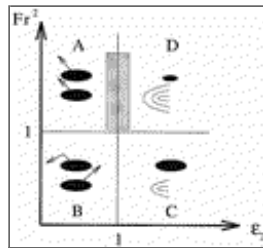
[Click on thumbnail for full-sized image.](#)

Figures



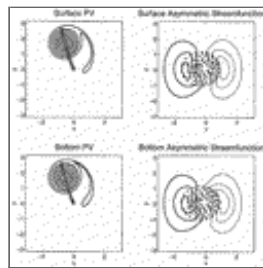
[Click on thumbnail for full-sized image.](#)

Fig. 1. The initial vortex. The streamfunction is shown at top, with contour interval $CI = \pm[0.1:0.1:1]$; the vorticity is in the middle panel, with $CI = \pm[1:1:10]$; and the azimuthal velocity profile at bottom. The bold contours are negative values, the thin are positive.



[Click on thumbnail for full-sized image.](#)

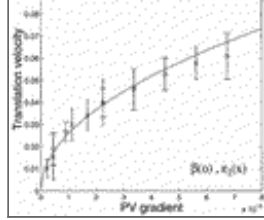
Fig. 2. A schematic of the results for the initially barotropic vortex. The x axis is the nondimensional slope parameter, and the y axis is the (squared) ratio of vortex radius to the deformation radius. The cases A, B, etc., are labeled in order of appearance in the text.



[Click on thumbnail for full-sized image.](#)

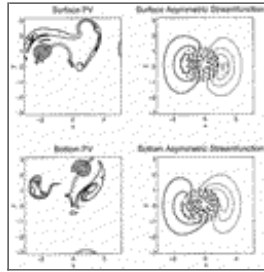
Fig. 3. The two-layer vortex with $r_0 = 2.5\lambda$ and $\epsilon_2 = 0.02$. At left are the potential vorticities at $t = 37.5$ ($CI = \pm[0.5, 1:1:10]$); at right are the asymmetric streamfunction fields at $t = 5$ ($CI = \pm[0.025, 0.05, 0.1:0.1:1]$) with the actual streamfunction superimposed with dashed lines ($CI = \pm[0.008:0.008:0.08]$). The PV centroid positions are shown every two time units in the left plots. All terms are defined in the text and the slope is shallowing toward the top of the figures. In this and all similar figures, the center of the vortex is initially $x = 0, y = 0$.





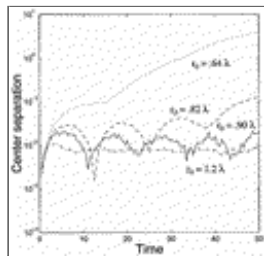
Click on thumbnail for full-sized image.

Fig. 4. The translation velocity obtained from fits of $[x(t), y(t)]$ for the one- and a two-layer vortex with $r_0 = 2.5\lambda$. The “x” indicates the two-layer velocity, the “O” the one-layer velocity. β_2 has been scaled by a factor of 2 for the comparison—see text. The solid curve varies as $\beta^{1/2}$. The error bars are from the least square fits of the vortex position in time.



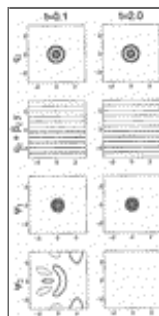
Click on thumbnail for full-sized image.

Fig. 5. The two-layer vortex with $r_0 = 0.64\lambda$ and $\epsilon_2 = 0.02$. At left are the PV fields at $t = 45$ and at right, the asymmetric streamfunction fields at $t = 5$ (with actual streamfunction superimposed with dashed lines). The contour intervals are the same as in the figure with the $r_0 = 2.5\lambda$ vortex. The PV centroid positions are again drawn every two time units.



Click on thumbnail for full-sized image.

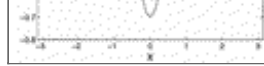
Fig. 6. The distance between the potential vorticity-weighted centers of the upper and lower portions of the vortex with $\epsilon_2 = 0.02$. The vortex sizes are as labeled, and centers calculated as indicated in the text.



Click on thumbnail for full-sized image.

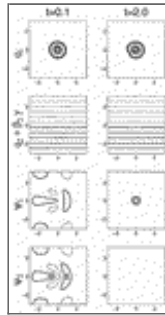
Fig. 7. The fields for the two-layer vortex with $r_0 = 0.64\lambda$ and $\epsilon_2 = 36$ at $t = 0.1$ and $t = 2$. The initial fields, not shown, are identical to those in cases A and B; that is, they are barotropic. The upper PV CI = $\pm[1:1:10]$, the bottom PV CI = $\pm[0.3, 0.9, 1.5, 2.1, 2.7]$, and the streamfunction CI = $\pm[0.1:0.1:1]$. The $t = 2$ fields are averaged from three realizations, at $t = 1.9, 2, 2.1$.





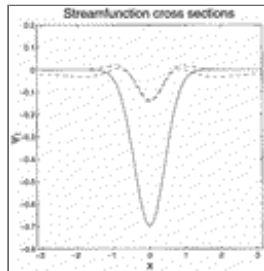
[Click on thumbnail for full-sized image.](#)

Fig. 8. The initial and final streamfunction with that predicted by a linear evolution; the $r_0 = 0.64\lambda$ vortex with $\epsilon_2 = 36$. The CI = $\pm[0.1,0.1,1]$. The $t = 2$ fields are averaged from three realizations, at $t = 1.9, 2, 2.1$. In the cross-section plot, the solid curve is the initial vortex, the dashed curve is the vortex at $t = 2$ and the dash-dot curve is the predicted profile.



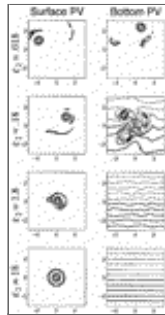
[Click on thumbnail for full-sized image.](#)

Fig. 9. The fields for the two-layer vortex with $r_0 = 2.5\lambda$ at $t = 0.1$ and $t = 2$. The upper PV CI = $\pm[1:1:10]$, the bottom PV CI = $\pm[0.3,0.9,1.5,0.2,1,2.7]$, and the streamfunction CI = $\pm[0.1:0.1:1]$. The $t = 2$ fields are averaged from three realizations, at $t = 1.9, 2, 2.1$.



[Click on thumbnail for full-sized image.](#)

Fig. 10. The initial and final streamfunction with that predicted by a linear evolution, for the $r_0 = 2.5\lambda$ vortex with $\epsilon_2 = 36$. The CI = $\pm[0.05,0.05,0.5]$. The $t = 2$ fields are averaged from three realizations, at $t = 1.9, 2, 2.1$. In the cross-section plot, the solid curve is the initial vortex, the dashed curve is the vortex at $t = 2$, and the dash-dot curve is the predicted profile.



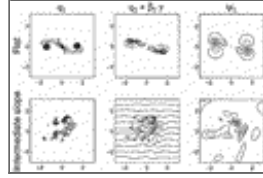
[Click on thumbnail for full-sized image.](#)

Fig. 11. The upper and lower potential vorticity for the $r_0 = 0.64\lambda$ vortex with various bottom slopes. The upper PV CI = $\pm[1:1:10]$ for q_1 and bottom PV CI were chosen to yield 15 contours in the range of the minimum and maximum values of $q_2 + \beta_2 y$. The corresponding times are $t = 45$ ($\epsilon_2 = 0.018$), $t = 20$ ($\epsilon_2 = 0.18$), $t = 4$ ($\epsilon_2 = 1.8$), and $t = 0.5$ ($\epsilon_2 = 18$).



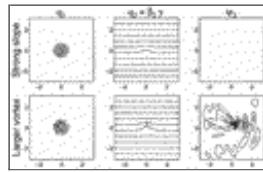
[Click on thumbnail for full-sized image.](#)

Fig. 12. The upper and lower potential vorticity for the $r_0 = 2.5\lambda$ vortex with various bottom slopes. The $CI = \pm[1:1:10]$ for q_1 and the bottom PV CI were chosen to yield 15 contours in the range of the minimum and maximum values of $q_2 + \beta_2 y$. The corresponding times are $t = 37.5$ ($\epsilon_2 = 0.018$), $t = 20$ ($\epsilon_2 = 0.18$), $t = 10$ ($\epsilon_2 = 1.8$), and $t = 0.5$ ($\epsilon_2 = 0.018$).



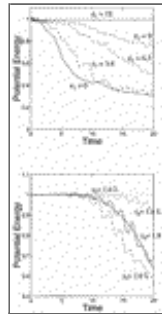
[Click on thumbnail for full-sized image.](#)

Fig. 13. A surface-trapped vortex ($\psi_1 = -0.7 \exp(-r^2 / (2r_0^2))$), and $\psi_2 = 0$ with $r_0 = 2.5\lambda$ over a flat bottom and an intermediate slope ($\epsilon_1 = 3.6$) at a late time ($t = 15$). At left is the surface PV, with contour intervals $\pm[5:5:50]$, in the middle the bottom PV with $CI = \pm[0.3,0.9,1.5,2.1,2.7]$, and at right the bottom streamfunction, with $CI = \pm[0.1:0.1:0.4]$.



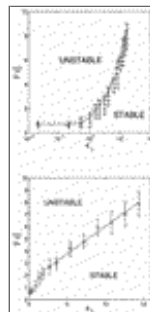
[Click on thumbnail for full-sized image.](#)

Fig. 14. The same vortex ($r_0 = 2.5\lambda$) with a stronger slope ($\epsilon_1 = 18$) and a larger vortex ($r_0 = 4.2\lambda$) over the same slope, also at $t = 15$. The contour intervals are as in the previous figure, except for those of the deep streamfunction, which are $CI = \pm [0.025:0.025:0:1]$ (due to the weak flow).



[Click on thumbnail for full-sized image.](#)

Fig. 15. Potential energy as a function of time for a vortex with $r_0 = 2.5\lambda$ over various bottom slopes (upper panel) and one over a fixed slope ($\epsilon_1 = 3.6$) with various sizes of initial vortex (lower panel). The smoothed curve in the bottom figure is an example of the cubic fit used in the construction of the next figure (see text).



[Click on thumbnail for full-sized image.](#)

Fig. 16. Curves of “marginal stability” for the surface Gaussian vortex. The upper panel shows the curves for $PE(t = 20)/PE(t = 0) = 0.95$ (solid) and 0.8 (dashed); the circles indicate parameters of the experiments. In the lower graph are the positions of the $PE(t = 20)/PE(t = 0) = 0.95$ points, with error bars from the estimates derived from a cubic spline fitting of the data.

* WHOI Contribution Number 9580.

Corresponding author address: Joe LaCasce, Woods Hole Oceanographic Institution, M.S. 29, Woods Hole, MA 02543.


E-mail: jlacasse@whoi.edu

¹ Using a minimum PV cutoff yields a centroid indicative of the position of the vortex core, and avoids contributions from neighboring PV.

² The vortices are aligned to perform the subtraction using the final and initial PV centroids, as defined above. The amplitude of the streamfunction is scaled down, by a small fraction, because the vortex is slightly weakened by the cross-slope motion.

³ Such translation does not last forever because a barotropic vortex must disperse eventually into Rossby waves. However, a period of translation at a constant velocity is often found numerically (e.g., [Fiorini and Elsberry 1989](#)) and analytically (e.g., [Reznik and Dewar 1994](#)).

⁴ The slope gradient from the stratified case has been scaled for comparison with that from the barotropic case because $\beta_2 = f\partial_y H/H_2 = (1 + H_1/H_2)j\partial_y H/H = (1 + H_1/H_2)\beta$.

⁵ The sponge, a filter function of the form $sponge = 0.5 + 0.25\{\tanh[(x - 0.3)/10] + \tanh[2\pi - x + 0.3)/10]\}$, was convolved with the lower-layer perturbation PV field at each time step, thereby decreasing the field at the left and right edges of the domain. The filter, which is unity at the center of the domain and decays to 0.5 at the left and right edges, was chosen (empirically) as a compromise to weaken the waves and not to support reflected waves. As is discussed below, the waves have zero surface PV, so it is not necessary to damp that field. The sponge is only partially successful at removing waves. Thus the $t = 2$ fields in [Figs. 7](#)  have been averaged from those found at $t = 1.9, 2, 2.1$ to filter the residual waves.

⁶ Note this is the same size vortex as that used in barotropic cases A and D.

⁷ By conservation of energy and assuming a complete conversion of potential to kinetic energy, one has $PE(t_0) + KE_1(t_0) \approx KE_1(t_p) + KE_2(t_p) \approx 2KE_1(t_p)$. If moreover the vortex is roughly deformation scale, $PE(t_0) \approx KE_1(t_0)$, which yields $U_2(t_p) \approx U_1(t_0)$. The vortex in the example is larger than deformation scale, which favors stronger final flows.

⁸ The instability at $\epsilon_1 = O|1|$ is predominantly radiating, that is, topographic waves are generated rather than vortices. As such, the unstable modes are wavelike, as in the so-called radiating instability on the β plane (see [Kamenkovich and Pedlosky, 1996](#), and references therein). In the presence of a mean PV gradient, one finds both “trapped” and radiating unstable modes, and a stronger gradient favors the radiating modes. The latter yield a faster means of spreading kinetic energy laterally and, thus, have been invoked as a mechanism to explain variability far from unstable currents.

⁹ I have omitted a deep estimate for the North Brazil eddy because it appears that these features are formed over topography, rather than colliding with a slope, as in the other cases.

top ▲



© 2008 American Meteorological Society [Privacy Policy and Disclaimer](#)
Headquarters: 45 Beacon Street Boston, MA 02108-3693
DC Office: 1120 G Street, NW, Suite 800 Washington DC, 20005-3826
amsinfo@ametsoc.org Phone: 617-227-2425 Fax: 617-742-8718
[Allen Press, Inc.](#) assists in the online publication of AMS journals.